Compressed Sensing for High Resolution 3D Photoacoustic Tomography

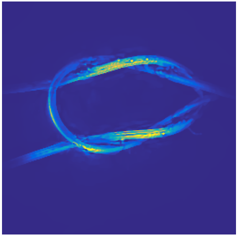

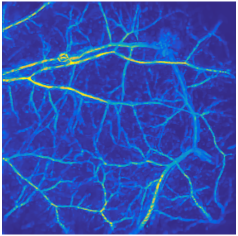

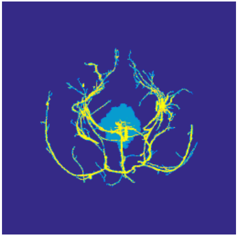

Felix Lucka
University College London
f.lucka@ulc.ac.uk

joint with:
Simon Arridge, Paul Beard, Marta Betcke,
Ben Cox, Nam Huynh & Edward Zhang

Centre for Medical Image Computing

INdAM Workshop on Biomedical Imaging
Rome, Feb 09, 2017.

UCL CENTRE FOR INVERSE PROBLEMS

Optical Part

chromophore concentration: c_k

optical absorption coefficient: $\mu_a(c)$

Acoustic Part

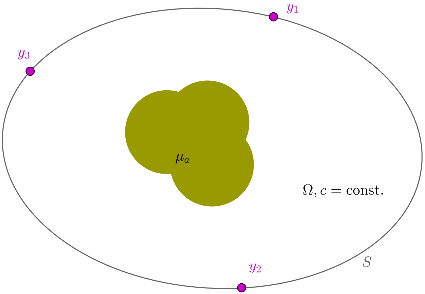

Photoacoustic Imaging: Basic Principles

Optical Part

chromophore concentration: c_k

optical absorption coefficient: $\mu_a(c)$

pulsed laser excitation: $\Phi(\mu_a)$

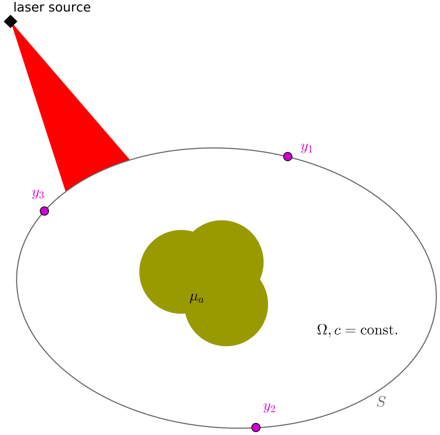

Acoustic Part

Photoacoustic Imaging: Basic Principles

Optical Part

chromophore concentration: c_k

optical absorption coefficient: $\mu_a(c)$

pulsed laser excitation: $\Phi(\mu_a)$

thermalization: $H = \mu_a \Phi(\mu_a)$

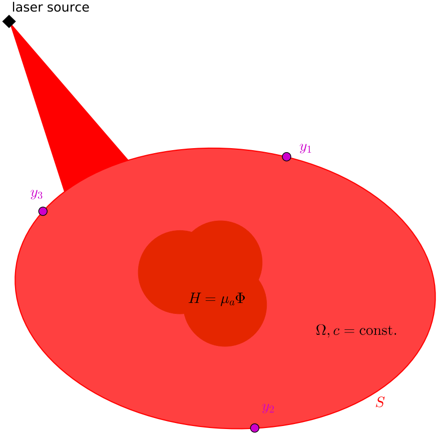

Acoustic Part

Optical Part

chromophore concentration: c_k

optical absorption coefficient: $\mu_a(c)$

pulsed laser excitation: $\Phi(\mu_a)$

thermalization: $H = \mu_a \Phi(\mu_a)$

Acoustic Part

local pressure increase: $p_0 = \Gamma H$

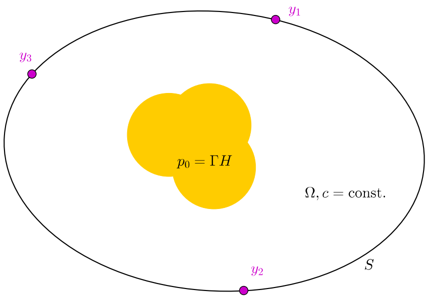

Optical Part

chromophore concentration: c_k

optical absorption coefficient: $\mu_a(c)$

pulsed laser excitation: $\Phi(\mu_a)$

thermalization: $H = \mu_a \Phi(\mu_a)$

Acoustic Part

local pressure increase: $p_0 = \Gamma H$

elastic wave propagation:

$$\Delta p - \frac{1}{c^2}\frac{\partial^2 p}{\partial^2 t} = 0$$

$$p|_{t=0} = p_0, \quad \frac{\partial p}{\partial t}|_{t=0} = 0$$

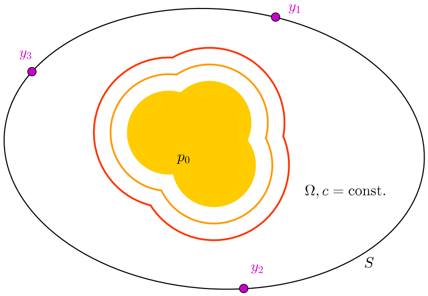

Optical Part

chromophore concentration: c_k

optical absorption coefficient: $\mu_a(c)$

pulsed laser excitation: $\Phi(\mu_a)$

thermalization: $H = \mu_a \Phi(\mu_a)$

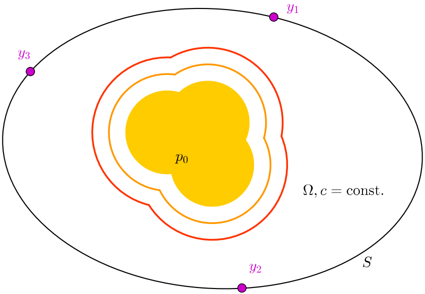

Acoustic Part

local pressure increase: $p_0 = \Gamma H$

elastic wave propagation:

$$\Delta p - \frac{1}{c^2}\frac{\partial^2 p}{\partial^2 t} = 0$$

$$p|_{t=0} = p_0, \quad \frac{\partial p}{\partial t}|_{t=0} = 0$$

measurement of pressure time courses:

$$f_i(t) = p(y_i, t)$$

Optical Part

chromophore concentration: c_k

optical absorption coefficient: $\mu_a(c)$

pulsed laser excitation: $\Phi(\mu_a)$

thermalization: $H = \mu_a \Phi(\mu_a)$

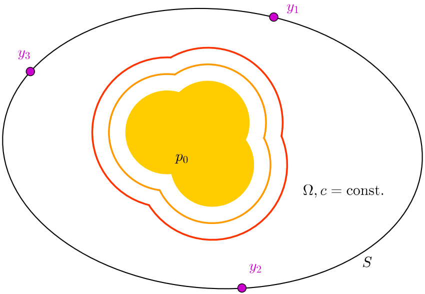

Acoustic Part

local pressure increase: $p_0 = \Gamma H$

elastic wave propagation:

$$\Delta p - \frac{1}{c^2}\frac{\partial^2 p}{\partial^2 t} = 0$$

$$p|_{t=0} = p_0, \quad \frac{\partial p}{\partial t}|_{t=0} = 0$$

measurement of pressure time courses:

$$f_i(t) = p(y_i, t)$$

Photoacoustic effect

- coupling of optical and acoustic modalities.
- "hybrid imaging"
- high optical contrast can be read by high-resolution ultrasound.

Photoacoustic Imaging: Basic Principles

Optical Part

chromophore concentration: c_k

optical absorption coefficient: $\mu_a(c)$

pulsed laser excitation: $\Phi(\mu_a)$

thermalization: $H = \mu_a \Phi(\mu_a)$

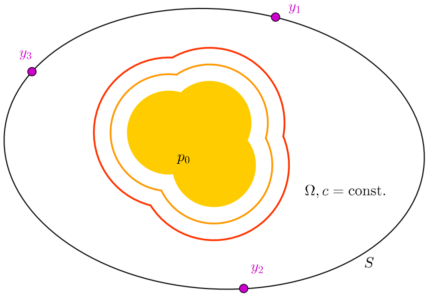

Acoustic Part

local pressure increase: $p_0 = \Gamma H$

elastic wave propagation:

$$\Delta p - \frac{1}{c^2} \frac{\partial^2 p}{\partial^2 t} = 0$$

$$p|_{t=0} = p_0, \quad \frac{\partial p}{\partial t}|_{t=0} = 0$$

measurement of pressure time courses:

$$f_i(t) = p(y_i, t)$$

Inverse problems:

! optical inversion (μ_a) from boundary data: severely ill-posed.

Photoacoustic Imaging: Basic Principles

Optical Part

chromophore concentration: c_k

optical absorption coefficient: $\mu_a(c)$

pulsed laser excitation: $\Phi(\mu_a)$

thermalization: $H = \mu_a \Phi(\mu_a)$

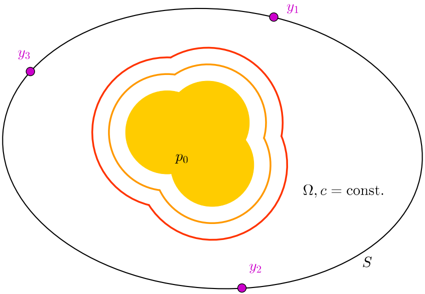

Acoustic Part

local pressure increase: $p_0 = \Gamma H$

elastic wave propagation:

$$\Delta p - \frac{1}{c^2}\frac{\partial^2 p}{\partial^2 t} = 0$$

$$p|_{t=0} = p_0, \qquad \frac{\partial p}{\partial t}|_{t=0} = 0$$

measurement of pressure time courses:

$$f_i(t) = p(y_i, t)$$

Inverse problems:

! optical inversion (μ_a) from boundary data: severely ill-posed.

✓ acoustic inversion (p_0) from boundary data: moderately ill-posed.

✓ optical inversion (μ_a) from internal data: moderately ill-posed.

Acoustic Inversion: The Spherical Radon Transform

$$\Delta p - \frac{1}{c^2}\frac{\partial^2 p}{\partial^2 t} = 0$$

$$p|_{t=0} = p_0, \quad \frac{\partial p}{\partial t}|_{t=0} = 0$$

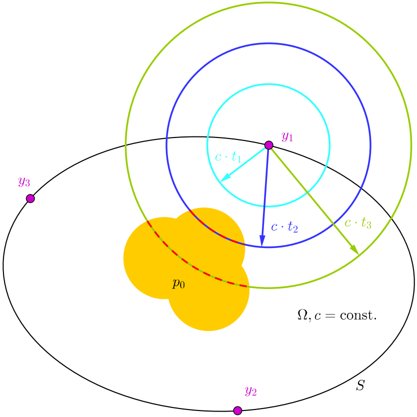

Poisson-Kirchhoff formula:
The measured signal g at a sensor at time t can be derived from the sum of all waves starting from a circle with radius $r = c \cdot t$:

$$f(y,t) = C\frac{\partial}{\partial_t} t \int_{B_{ct}} p_0(x)\mathrm{d}x$$
$$:= C\frac{\partial}{\partial_t} t\mathcal{M}p_0$$

$\mathcal{M}$ is called the spherical Radon transform.

$\Longrightarrow$ PAT inversion is basically a problem of integral geometry.

$\Longrightarrow$ Connections to Fourier analysis.

A *phase space point* (x, ξ) is said to be "visible" ("audible"), if a ray through x in the direction of ξ hits a sensor within the measurement time.

"Visibility region": All points x such that (x, ξ) is visible for all ξ.

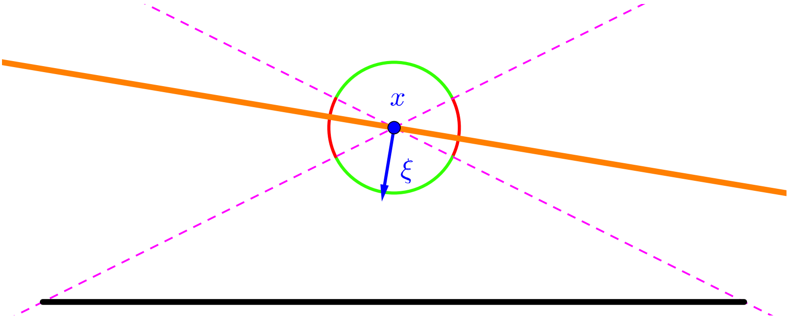

A *phase space point* (x, ξ) is said to be "visible" ("audible"), if a ray through x in the direction of ξ hits a sensor within the measurement time.

"Visibility region": All points x such that (x, ξ) is visible for all ξ.

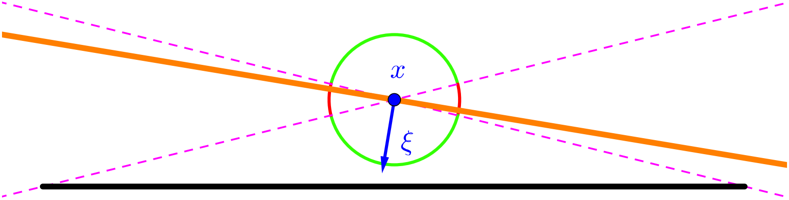

A *phase space point* (x, ξ) is said to be "visible" ("audible"), if a ray through x in the direction of ξ hits a sensor within the measurement time.

"Visibility region": All points x such that (x, ξ) is visible for all ξ.

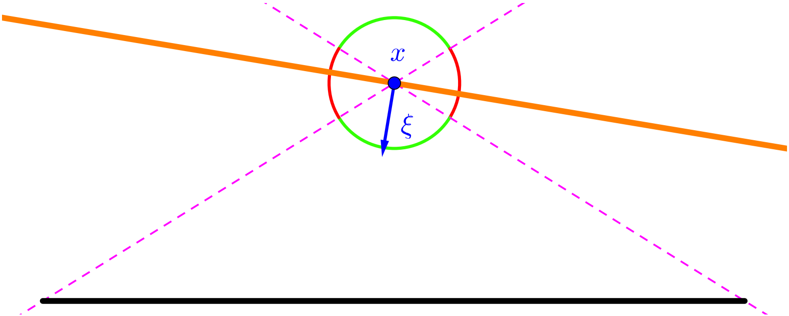

A *phase space point* (x, ξ) is said to be "visible" ("audible"), if a ray through x in the direction of ξ hits a sensor within the measurement time.

"Visibility region": All points x such that (x, ξ) is visible for all ξ.

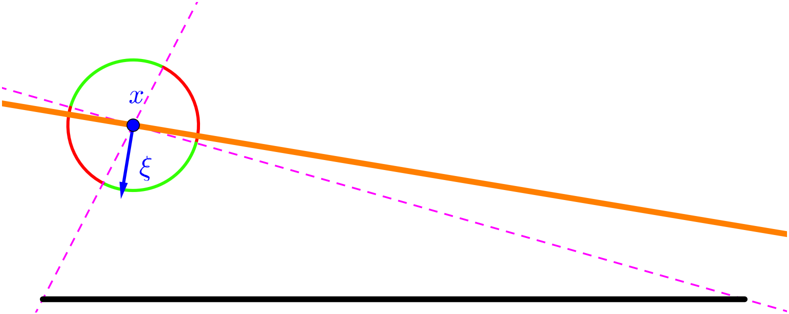

A *phase space point* (x, ξ) is said to be "visible" ("audible"), if a ray through x in the direction of ξ hits a sensor within the measurement time.

"Visibility region": All points x such that (x, ξ) is visible for all ξ.

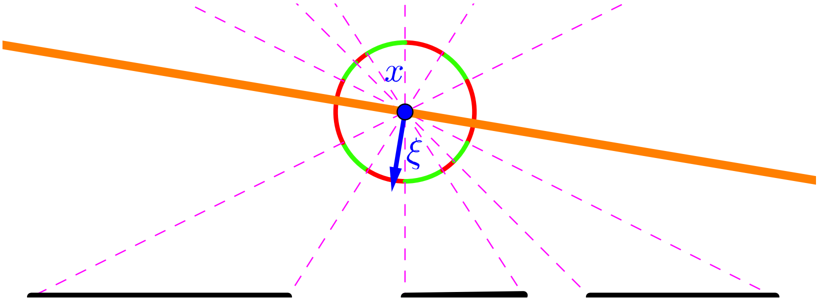

Photoacoustic Imaging: Applications

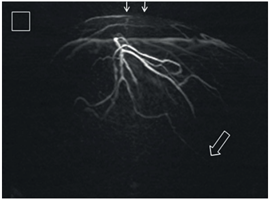

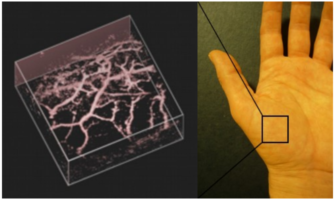

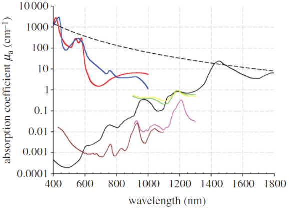

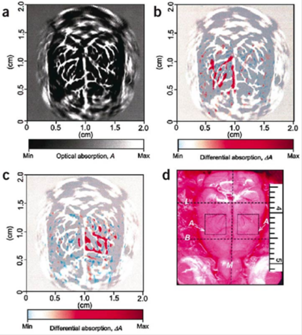

- High contrast between blood and water/lipid.
- Light-absorbing structures in soft tissue.
- Gap between oxygenated and deoxygenated blood.
- Different wavelengths allow quantitative spectroscopic examinations.
- Use of contrast agents for molecular imaging.
- Extremely promising future imaging technique!

sources: **Paul Beard, 2011**. *Biomedical photoacoustic imaging*, *Interface Focus.* Wikimedia Commons

Photoacoustic Sensing Systems

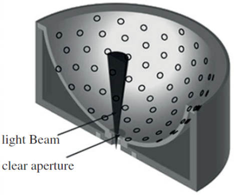

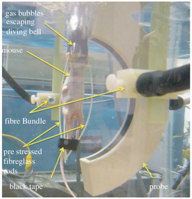

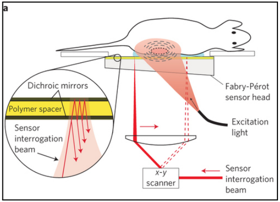

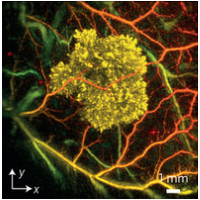

from: **Beard, 2011**, *Interface Focus*; **Jathoul et al., 2015**, *Nature Photonics*

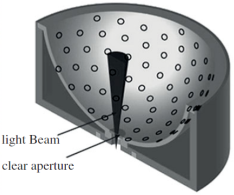

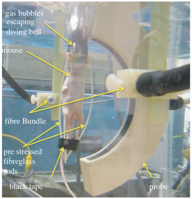

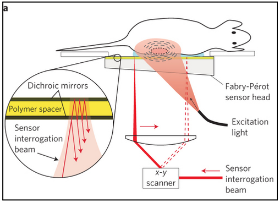

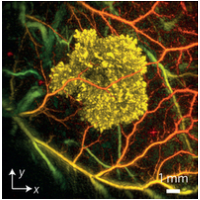

from: **Beard, 2011**, *Interface Focus*; **Jathoul et al., 2015**, *Nature Photonics*

- High res 3D PA images require sampling acoustic waves with a frequency content in the tens of MHz over cm scale apertures.
- Nyquist criterion results in tens of µm scale sampling intervals $\Longrightarrow$ several thousand detection points.
- Sequential scanning currently takes several minutes.
- Crucial limitation for clinical, spectral and dynamical PAT (4D PAT).

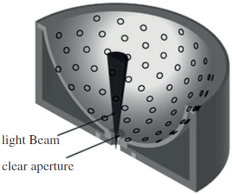

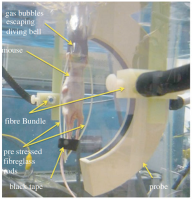

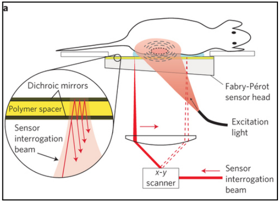

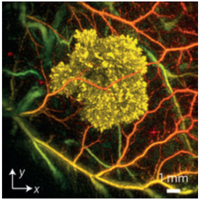

from: **Beard, 2011**, *Interface Focus*; **Jathoul et al., 2015**, *Nature Photonics*

Key observation and idea:

- Nyquist is too conservative (only band-limitlessness is assumed).
- Typical targets have additional structure, e.g., low spatial complexity (sparsity).
- Regularly sampled data is highly redundant.
- Non-redundant part could be sensed faster.
- Accelerated acquisition without significant loss of image quality.

Established as compressed sensing, successful in similar modalities.

Novel Fabry-Pérot-Based Sensing Systems

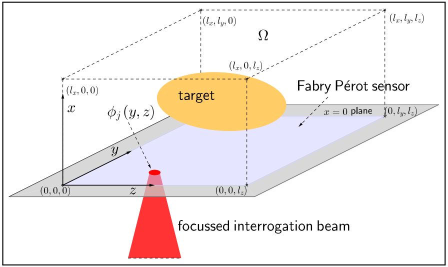

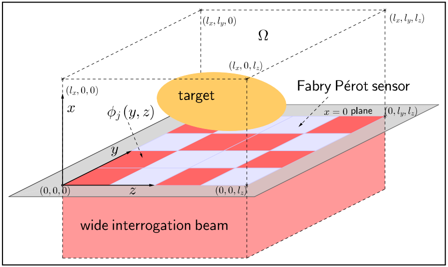

$$f_j(t) = \int p(x = 0, y, z, t)\phi_j(y, z)\, \mathrm{d}y\mathrm{d}z$$

- Single-point sub-sampling (structured or random).
- Patterned interrogation similar to "single-pixel" Rice camera (via micromirror array).
- Multi-beam scanning + sub-sampling.

Applicable to other sequential scanning schemes, see **Huynh et al., 2014, 2015, 2016** for technical details.

Novel Fabry-Pérot-Based Sensing Systems

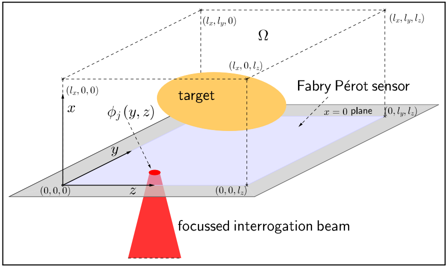

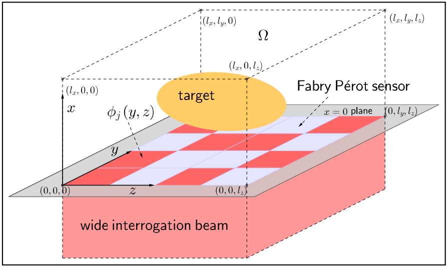

Image model: $$f_i^c = C_i f_i = C_i(Ap_i + \varepsilon_i)$$ for each frame i.

Image reconstruction:

- $f_i^c \longrightarrow f_i$, $f_i \longrightarrow p_i$ by standard method, frame-by-frame.
- $f_i^c \longrightarrow p_i$: standard or new method, frame-by-frame.
- $F^c \longrightarrow F$, $f_i \longrightarrow p_i$ by standard method, frame-by-frame.
- $F^c \longrightarrow P$: Full spatio-temporal method.

Novel Fabry-Pérot-Based Sensing Systems

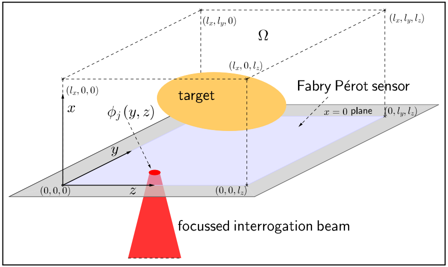

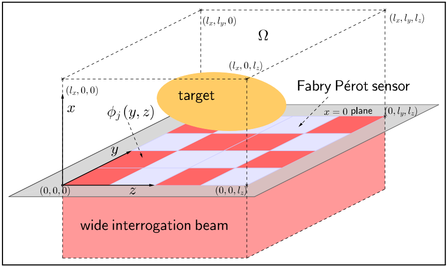

Image model: $$f_i^c = C_i f_i = C_i(Ap_i + \varepsilon_i)$$ for each frame i.

Image reconstruction:

- $f_i^c \longrightarrow f_i$, $f_i \longrightarrow p_i$ by standard method, frame-by-frame.
- $f_i^c \longrightarrow p_i$: standard or new method, frame-by-frame.
- $F^c \longrightarrow F$, $f_i \longrightarrow p_i$ by standard method, frame-by-frame.
- $F^c \longrightarrow P$: Full spatio-temporal method.

Standard Reconstruction & Numerical Wave Propagation

Analytic methods, e.g. eigenfunction expansion and closed-form filtered-backprojection, are too restrictive for us.

Time Reversal (TR):

- "Least restrictive PAT reconstruction"
- Sending the recorded waves "back" into volume.
- Requires a numerical model for acoustic wave propagation.

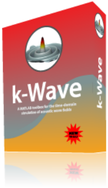

k-Wave♣ implements a *k*-space pseudospectral method to solve the underlying system of first order conservation laws:

- Compute spatial derivatives in Fourier space: 3D FFTs.
- Modify finite temporal differences by *k*-space operator and use staggered grids for accuracy and robustness.
- Perfectly matched layer to simulate free-space propagation.
- Parallel/GPU computing leads to massive speed-ups.

♣**B. Treeby and B. Cox, 2010**. *k-Wave: MATLAB toolbox for the simulation and reconstruction of photoacoustic wave fields*, *Journal of Biomedical Optics.*

A Realistic Numerical Phantom

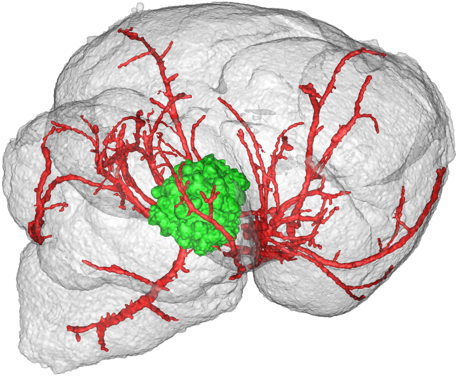

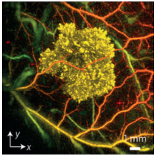

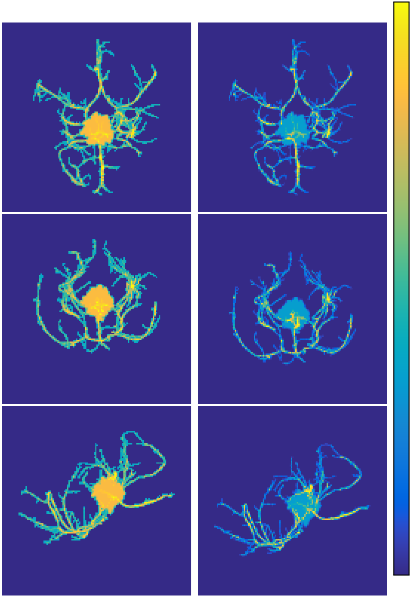

Time Reversal for Sub-Sampled Data

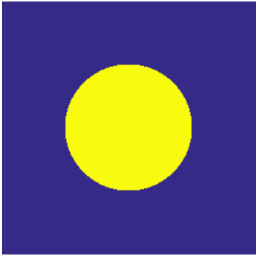

(a) IC, $n = 256^3$

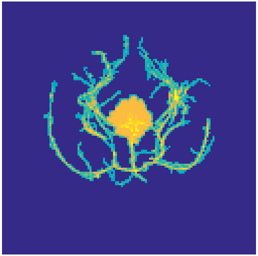

(b) high con., IC, $n = 128^3$

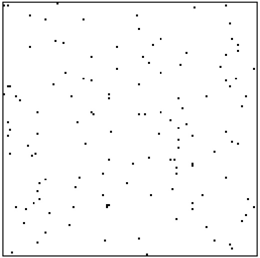

(c) sub-sampling, 128x

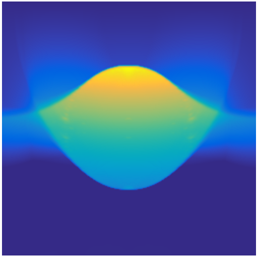

(d) TR 1

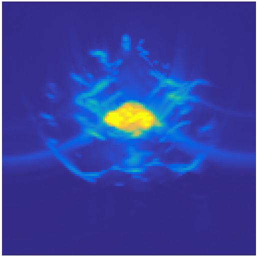

(e) TR 2

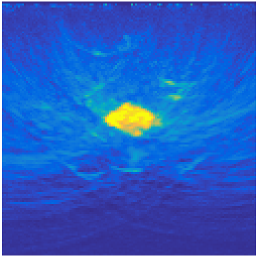

(f) TR 2, sub-sampled

sensor on top; inverse crime data sampled at Nyquist; max intensity proj., side view

Time Reversal for Sub-Sampled Data II

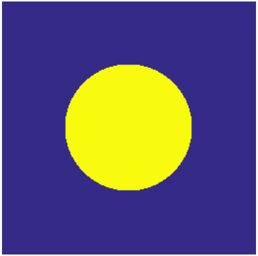

(a) IC, $n = 256^3$

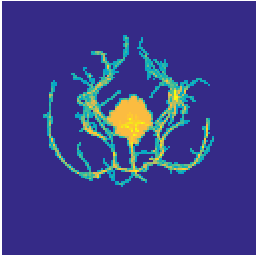

(b) high con., IC, $n = 128^3$

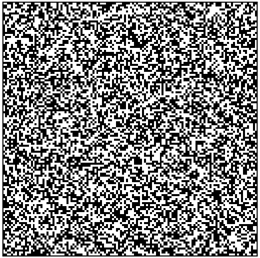

(c) sub-sampling, 1/128

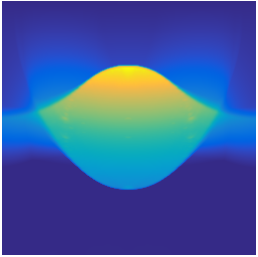

(d) TR 1

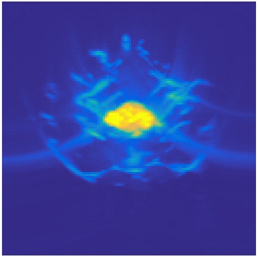

(e) TR 2

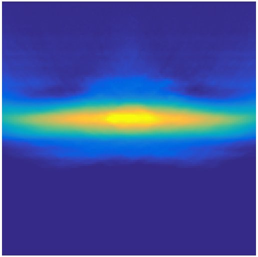

(f) TR 2, sub-sampled

sensor on top; inverse crime data sampled at Nyquist; max intensity proj., side view

Solving variational regularization problems

$$\hat{p} = \underset{p \geqslant 0}{\operatorname{argmin}} \left\{ \tfrac{1}{2} \| CAp - f^c \|_2^2 + \lambda \mathcal{J}(p) \right\}$$

iteratively by first-order methods requires implementation of A and A^*.

k-Wave yields a discrete representation A_κ. For A^*, one can

1) adjoint k-Wave iteration to obtain $(A_\kappa)^*$ (algebraic adjoint):

- ✓ high numerical accuracy.
- ! tedious derivation, specific for k-Wave, limited insights.

Huang, Wang, Nie, Wang, Anastasio, 2013. *IEEE Trans Med Imaging*

2) derive analytical adjoint and discretize it, e.g., $(A^*)_\kappa$.

- ✓ good numerical accuracy.
- ✓ simple proof, theoretical insights, generalizes to various numerical schemes.

Arridge, Betcke, Cox, L, Treeby, 2016.. *On the Adjoint Operator in Photoacoustic Tomography*, *Inverse Problems* 32(11).

Comparison for Conventional Data

$$\hat{p} = \underset{p \geqslant 0}{\operatorname{argmin}} \left\{ \frac{1}{2} \| Ap - f \|_2^2 + \lambda \mathcal{J}(p) \right\}$$

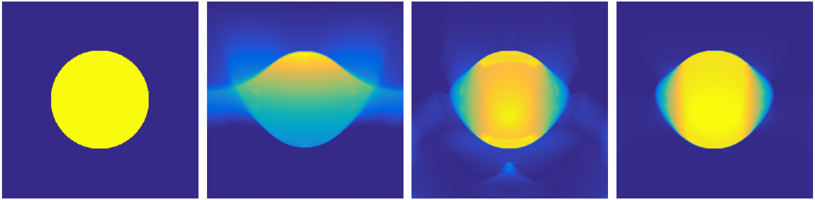

(a) $n = 256^3$ (b) TR (c) LS+ (d) TV+

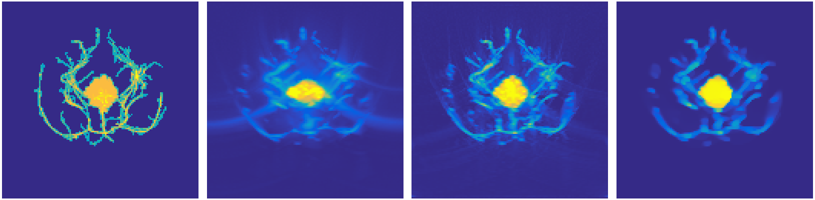

(e) $n = 128^3$ (f) TR (g) LS+ (h) TV+

sensor on top; inverse crime data sampled at Nyquist; max intensity proj., side view

Sub Sampled Data, Best Case Scenario

$$\hat{p} = \underset{p \geqslant 0}{\operatorname{argmin}} \left\{ \frac{1}{2} \| CAp - f^c \|_2^2 + \lambda \mathcal{J}(p) \right\}$$

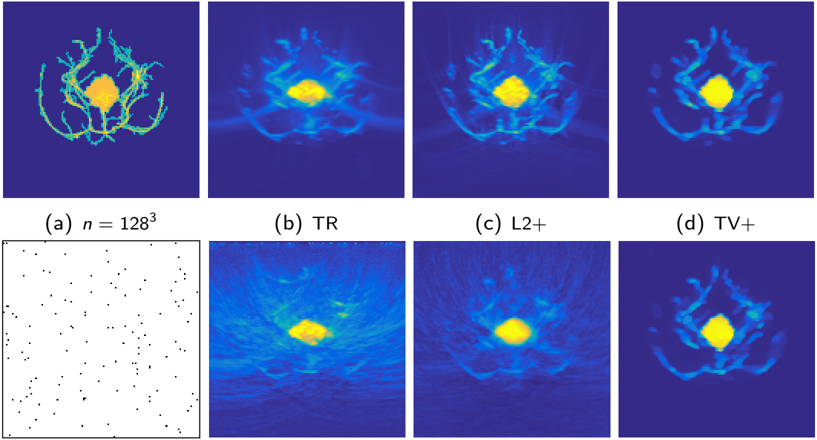

(a) $n = 128^3$ (b) TR (c) L2+ (d) TV+

(e) SubSam, 128x (f) TR (g) L2+ (h) TV+

sensor on top; inverse crime data sampled at Nyquist; max intensity proj., side view

Variational approaches,

$$\hat{p} = \operatorname*{argmin}_{p} \left\{ \tfrac{1}{2} \| CAp - f^c \|_2^2 + \lambda \mathcal{J}(p) \right\},$$

suffer from systematic bias (e.g., contrast loss for TV):

! Problem for quantitative use.

✓ Iterative enhancement trough Bregman iterations:

$$p^{k+1} = \operatorname*{argmin}_{p} \left\{ \frac{1}{2} \| CA\, p - (f^c + b^k) \|_2^2 + \lambda \mathcal{J}(p) \right\}$$
$$b^{k+1} = b^k + \left(f^c - CA\, p^{k+1} \right)$$

Potential for sub-sampling demonstrated in several other applications.

Osher, Burger, Goldfarb, Xu, Yin, 2006. *An iterative regularization method for total variation-based image restoration*, *Multiscale Modeling and Simulation*, 4(2):460-489.

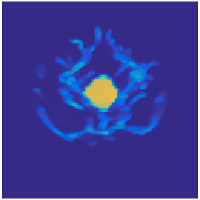

(a) TV+, cnv data

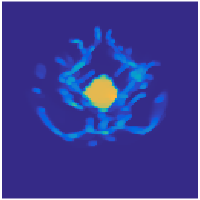

(b) TV+Br, cnv data

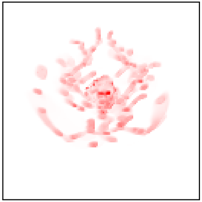

(c) $(p_{\text{TV+Br}} - p_{\text{TV+}})_+$, cnv data

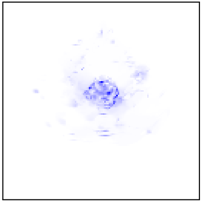

(d) $(p_{\text{TV+Br}} - p_{\text{TV+}})_-$, cnv data

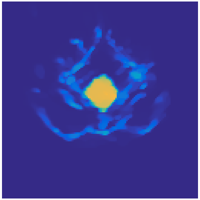

(e) TV+, rSP-128

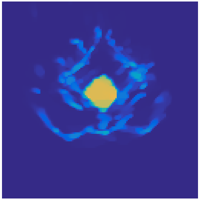

(f) TV+Br, rSP-128

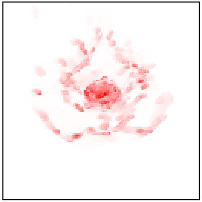

(g) $(p_{\text{TV+Br}} - p_{\text{TV+}})_+$, rSP-128

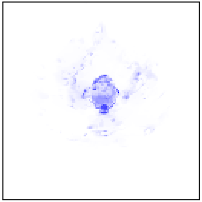

(h) $(p_{\text{TV+Br}} - p_{\text{TV+}})_-$, rSP-128

sensor on top; inverse crime data sampled at Nyquist; max intensity proj., side view

Inverse Crimes & Nyquist Rates

! Data created by the same forward model used for reconstruction.

! Conventional data was sampled at Nyquist rates in space and time.

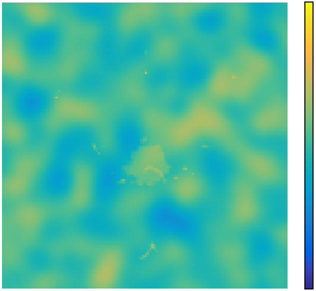

(a) $c_0 + \tilde{c}$ (b)

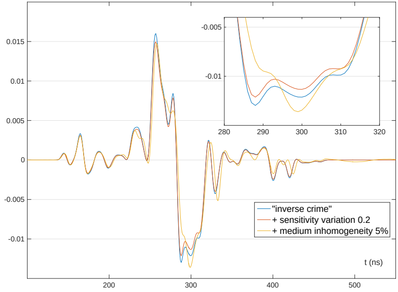

(c) pressure-time courses

To obtain more realistic results:

- Generate data with perturbed, heterogeneous acoustic model.
- Model inhomogenous sensitivity and noise level of sensor channels.
- Conventional, "full" data is acquired below spatial Nyquist rate.

Conventional data acquired on 2×2 too coarse grid.

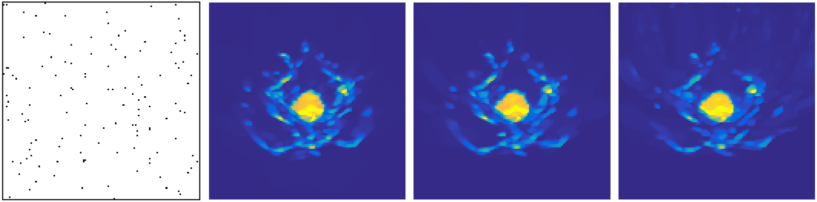

(d) single point (e) TV+Br, 1x (f) TV+Br, 8x (g) TV+Br, 32x

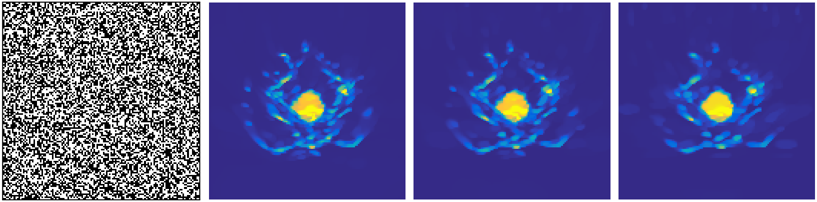

(h) patterned inter. (i) TV+Br, 1x (j) TV+Br, 8x (k) TV+Br, 32x

sensor on top; max intensity proj., side view

Leaving the Comfort Zone: Reproduction on Real Data

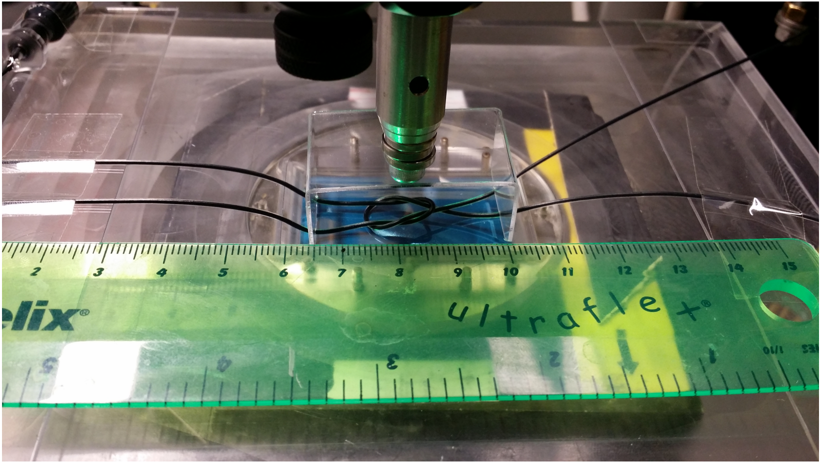

- Two polythene tubes filled with 10/100% ink.
- Stop-motion-style data acquisition of pulling one tube end.
- 45 frames (15min for conventional scanning per frame).
- Conventional data reconstructions to validate sub-sampling.

Conventional "Full" Data

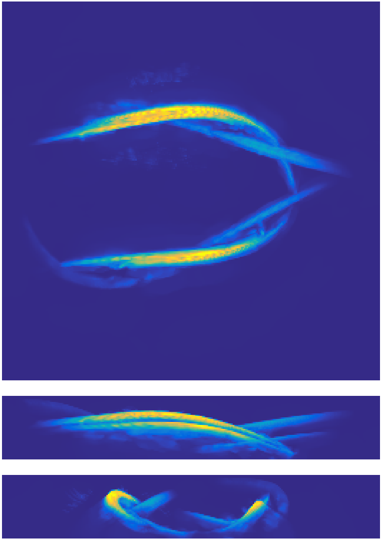

TR & TV denoising

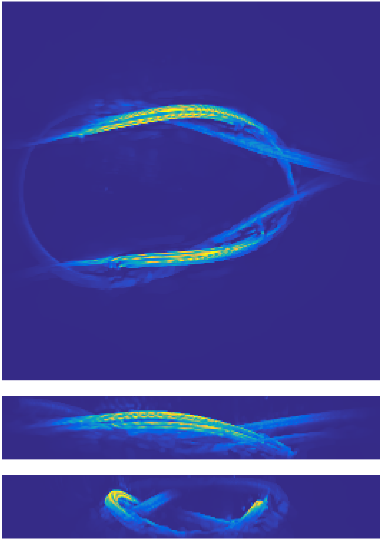

TV+

Random Point Sub-Sampled Data, 4x

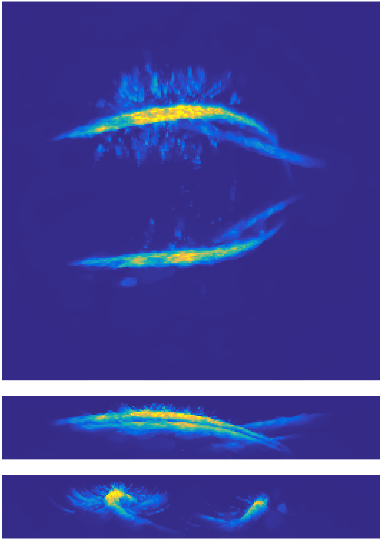

TR & TV denoising

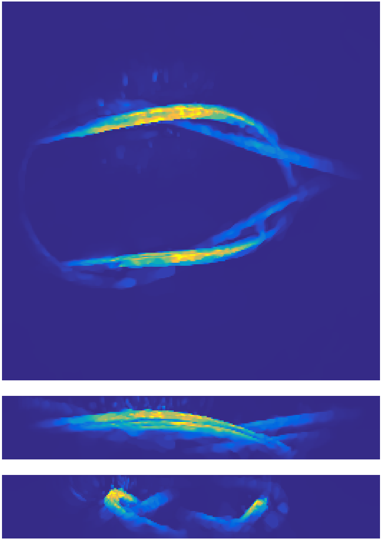

TV+

Random Point Sub-Sampled Data, 8x

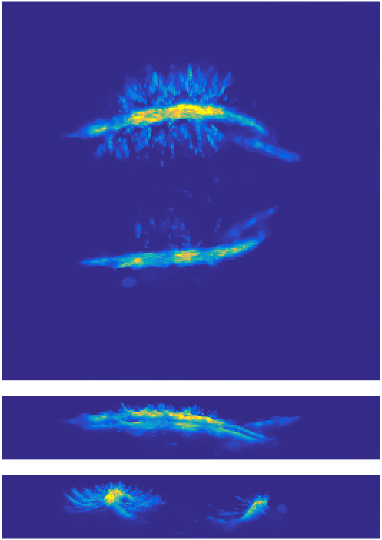

TR & TV denoising

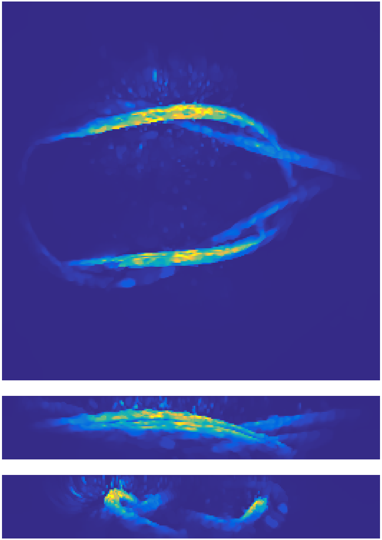

TV+

Random Point Sub-Sampled Data, 16x

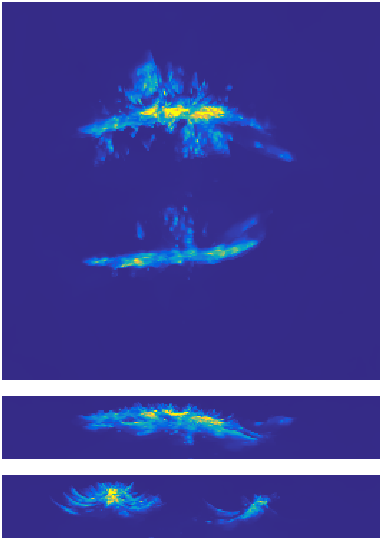

TR & TV denoising

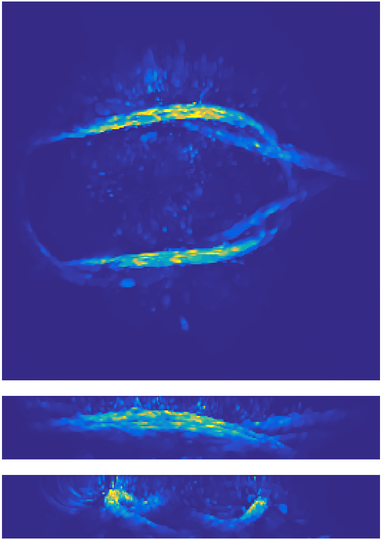

TV+

In Vivo Measurements: Conventional Data

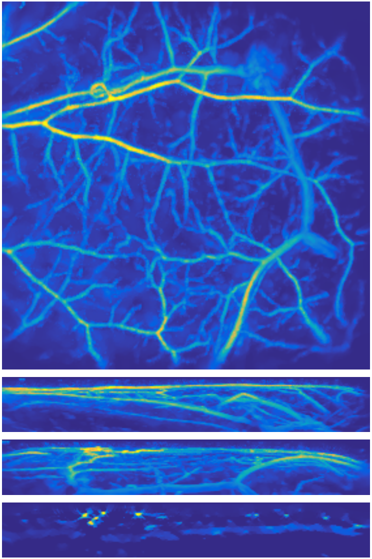

TR & TV denoising

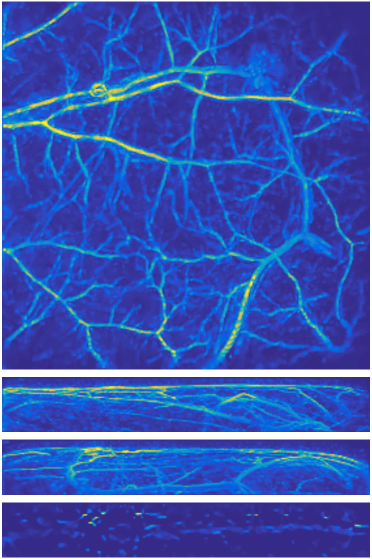

Bregman TV+

Thanks to Olumide Ogunlade for the excellent data!

In Vivo Measurements: 4x

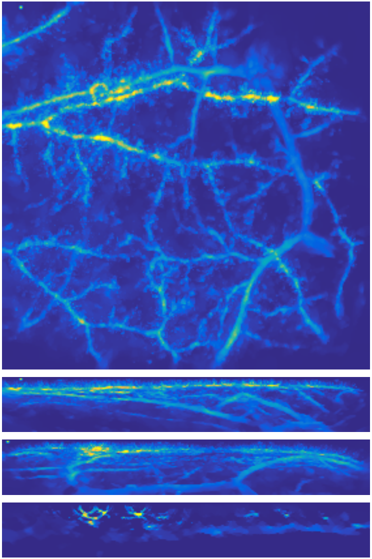

TR & TV denoising

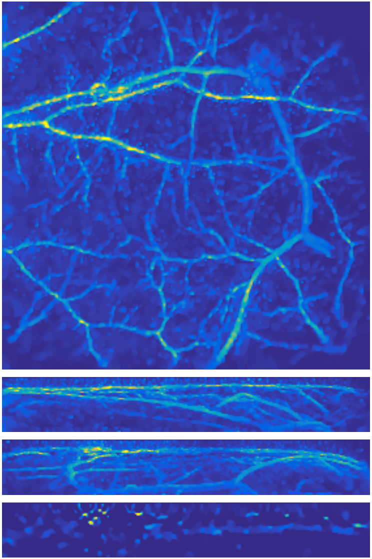

Bregman TV+

Thanks to Olumide Ogunlade for the excellent data!

In Vivo Measurements: 8x

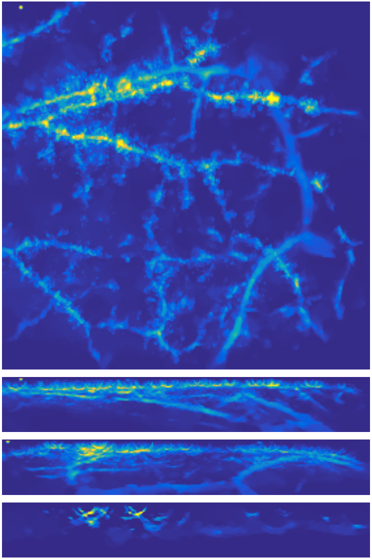

TR & TV denoising

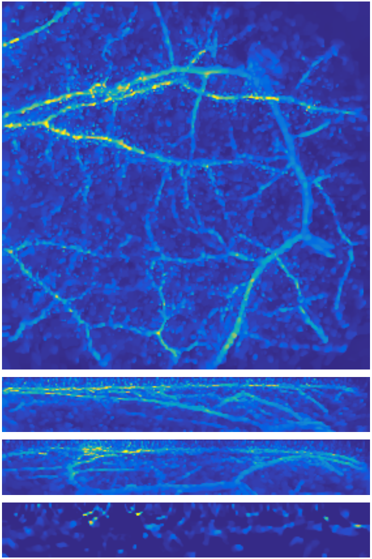

Bregman TV+

Thanks to Olumide Ogunlade for the excellent data!

Reaching a high acceleration through sub-sampling requires:

- Accurate model fit:
  - ! inhomogeneous optical excitation
  - ! uncertainty of acoustic parameters
  - ! inhomogeneity and defects of FP sensor
  - ! data artifacts by reflections / external sources

$\Longrightarrow$ Develop suitable, automatic pre-processing.
$\Longrightarrow$ Refine forward model used.

- Suitable regularization functionals:
  - ! TV is limited, especially for in-vivo data.
  - ! Experimental phantoms and in-vivo data are different.

$\Longrightarrow$ Develop suitable regularizing functionals.

Arridge, Beard, Betcke, Cox, Huynh, L, Ogunlade, Zhang, 2016. *Accelerated High-Resolution Photoacoustic Tomography via Compressed Sensing*, *Physics in Medicine and Biology* 61(24).

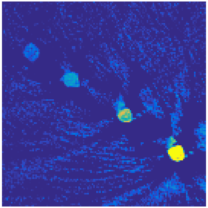

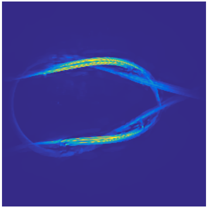

Continuous data acquisition

$\Longrightarrow$ tradeoff between spatial and temporal resolution.

Different dynamic models:

- Structured Low-Rank (functional imaging with static anatomies/QPAT).
- Tracer uptake/wash-in models.
- Perfusion models.
- Needle guidance
- Joint image reconstruction and motion estimation.

$$P = W \cdot V, \qquad P \in \mathbb{R}^{N \times K}, \ W \in \mathbb{R}^{N \times R}, \ V \in \mathbb{R}^{R \times K}, \ R \leqslant \min(N, K)$$

Example, $N = 10\,000$, $K = 25$, $R = 1$:

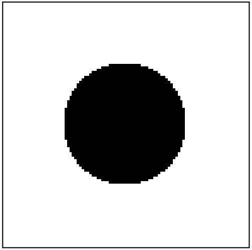

$W \in \mathbb{R}^{N \times 1}$

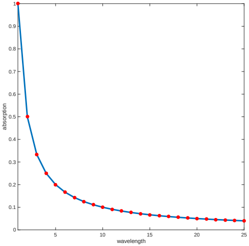

$V \in \mathbb{R}^{1 \times K}$

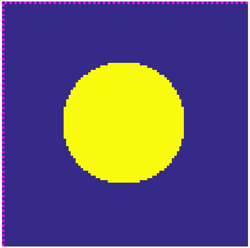

$P(\cdot, 1)$

Can we acquire multi-spectral data as fast as one conventional scan?

- spatial sub-sampling by factor $K = 25$.
- 4 instead of 100 scanning locations per wave length.
- geometric information scattered over data set.

$$\hat{p}_i = \underset{p \geqslant 0}{\operatorname{argmin}} \left\{ \| C_i A p - f_i^c \|_2^2 \right\} \quad \forall \; i = 1, \ldots, K$$

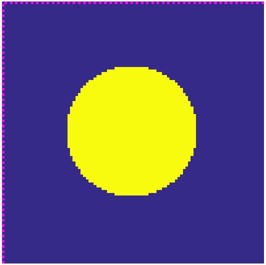

ground truth

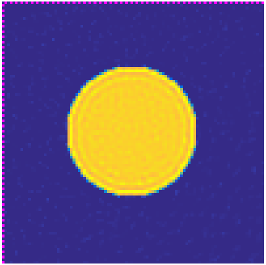

conventional data

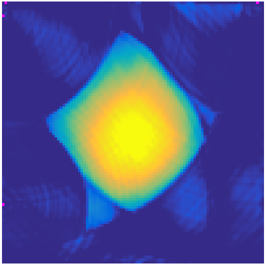

sub-sam. data

Neither geometry nor spectrum can be recovered!

Nuclear Norm Regularized Least Squares

$$\boxed{\hat{P} = \underset{P \geqslant 0}{\text{argmin}} \left\{ \tfrac{1}{2} \| CAP - F^c \|_{fro}^2 + \lambda |P|_* \right\}}, \qquad |B|_* = \sum_i \sigma_i(B) \quad (SVD)$$

λ such that $\text{rank}(P) = 1$ + Bregman iterations to restore contrast.

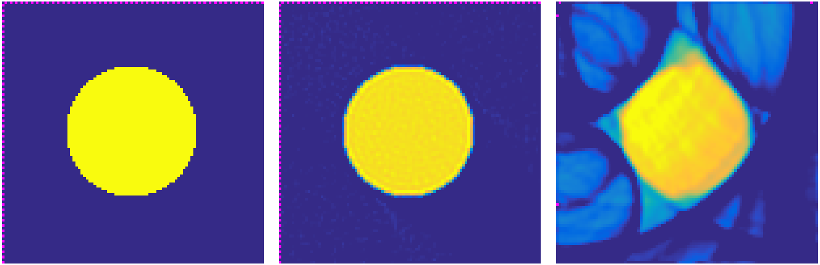

ground truth | conventional data | sub-sam. data

Better, but...

Iterative Least Squares with Non-Convex Projections

$$P^{k+1} = \Pi \left(P^k - \nu \nabla \tfrac{1}{2} \| CAP^k - F^c \|_2^2 \right) = \Pi \left(P^k - \nu A^T C^T \left(CAP^k - F^c \right) \right)$$

- ✓ Π projection onto convex set, e.g., $\mathbb{R}_+^N$.
- ✓ Π proximal mapping for convex functional, e.g., nuclear norm, TV.
- ! Π projection onto non-convex set, e.g., via non-negative matrix factorization: $\Pi(P) = \hat{W}\hat{V}$, where

$$(\hat{W}, \hat{V}) = \underset{W,V \geqslant 0}{\operatorname{argmin}} \| P - W\,V \|_2^2, \quad W \in \mathbb{R}^{N \times R}, V \in \mathbb{R}^{R \times K}$$

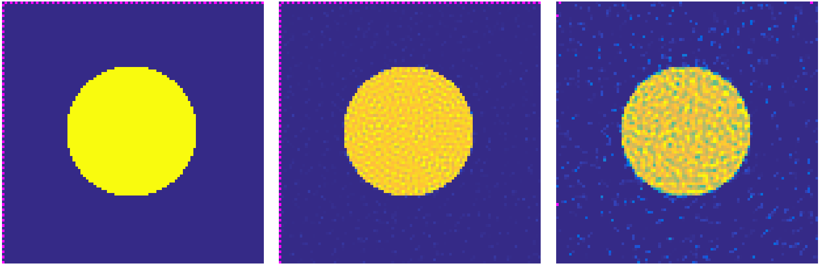

ground truth | conventional data | sub-sam. data

More General Dynamics

$$\hat{p}_i = \underset{p \geqslant 0}{\operatorname{argmin}} \left\{ \tfrac{1}{2} \| C_i A p - f_i^c \|_2^2 + \lambda TV(p) \right\}, \qquad \forall\ t = 1, \ldots, T$$

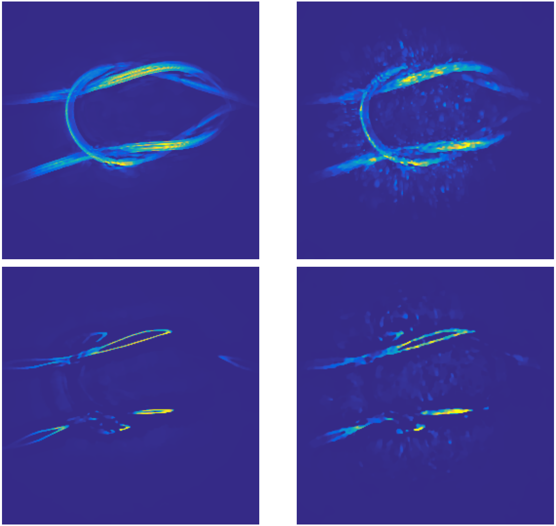

full data

sub-sampled data (16x)

Non-parametric spatio-temporal regularization: Find $P \in \mathbb{R}^{N \times T}$ as

$$\hat{P} = \underset{P \geqslant 0}{\operatorname{argmin}} \left\{ \sum_i^T \frac{1}{2} \| C_i A\, p_i - f_i^c \|_2^2 + \lambda \mathcal{R}(P) \right\},$$

Lot's of possibilities, here: Implicit model formulated as joint image and motion estimation:

$$(\hat{P}, \hat{V}) = \underset{P \geqslant 0, V}{\operatorname{argmin}} \left\{ \sum_i^T \frac{1}{2} \| C_i A\, p_i - f_i^c \|_2^2 + \alpha \mathcal{J}(p_i) + \beta \mathcal{H}(v_i) + \gamma \mathcal{S}(P, V) \right\}$$

$\mathcal{S}(P, V)$ enforces motion PDE, e.g., optical flow equation:

$$\partial_t p(x, t) + (\nabla_x p(x, t))\, v(x, t) = 0$$

Burger, Dirks, Schönlieb, 2016. *A Variational Model for Joint Motion Estimation and Image Reconstruction*, arXiv:1607.03255.

Example: TV-TV-Lp Regularization

$$\partial_t p(x,t) + (\nabla_x p(x,t))\, v(x,t) = 0$$

$\rightsquigarrow$ forward differences for ∂_t, central differences for ∇_x:

$$(\hat{P}, \hat{V}) = \underset{P \geqslant 0, V}{\operatorname{argmin}} \left\{ \sum_i^T \frac{1}{2} \| C_i A\, p_i - f_i^c \|_2^2 \right.$$
$$\left. + \alpha\, TV(p_i) + \beta\, TV(v_i) + \frac{\gamma}{p} \| (p_{i+1} - p_i) + (\nabla p_i) \cdot v_i \|_p^p \right\}$$

proximal-gradient-type scheme:

$$P^{k+1} = \mathbf{prox}_{\nu \mathcal{R}} \left(P^k - \nu A^T C^T \left(C A P^k - F^c \right) \right)$$

$$\mathbf{prox}_{\nu \mathcal{R}}(P) = \underset{Q \geqslant 0}{\operatorname{argmin}} \left\{ \frac{1}{2} \| Q - P \|_2^2 + \nu \mathcal{R}(Q) \right\}$$
$$= \underset{Q \geqslant 0}{\operatorname{argmin}} \left\{ \min_V \sum_i^T \frac{1}{2} \| q_i - p_i \|_2^2 \right.$$
$$\left. + \nu\alpha\, TV(q_i) + \nu\beta\, TV(v_i) + \frac{\nu\gamma}{p} \| (q_{i+1} - q_i) + (\nabla q_i) \cdot v_i \|_p^p \right\}$$

For $p \geqslant 1$, TV-TV-Lp denoising is a biconvex optimization problem:

$$\min_{Q \geqslant 0, V} S(Q, V) := \min_{Q \geqslant 0, V} \sum_i^T \frac{1}{2} \|q_i - p_i\|_2^2 + \nu\alpha TV(q_i) + \nu\beta TV(v_i) + \frac{\nu\gamma}{p} \|(q_{i+1} - q_i) + (\nabla q_i) \cdot v_i\|_p^p$$

Alternating optimization:

$$Q^{k+1} = \underset{Q}{\operatorname{argmin}}\, S(Q, V^k) \qquad \text{(TV-transport constr. denoising)}$$

$$V^{k+1} = \underset{V}{\operatorname{argmin}}\, S(Q^{k+1}, V) \qquad \text{(TV constr. optical flow estimation)}$$

! Both problems are convex but non-smooth.

! Need to ensure energy decrease.

! warm-start, over-relaxation, inertial, etc: difficult to validate.

Alternating optimization:

$$Q^{k+1} = \operatorname*{argmin}_{Q} S(Q, V^k) \qquad \text{(TV-transport constr. denoising)}$$

$$V^{k+1} = \operatorname*{argmin}_{V} S(Q^{k+1}, V) \qquad \text{(TV constr. optical flow estimation)}$$

Primal-dual hybrid gradient for both: Too slow convergence in 3D.

Alternating directions method of multipliers (ADMM):

- ! More difficult to parameterize (to ensure monotone energy).
- ! Badly conditioned, large-scale least-squares problems.
- ! Crucial: Choice of iterative solver, preconditioning and stop criterion.
- ✓ Overrelaxed ADMM with step size adaptation and CG solver for Q.
- ✓ Overrelaxed ADMM with AMG-CG solver for V (frame-by-frame).

Detailed evaluation in process!

A 2D Example: Frame-by-Frame Least Squares

$$\hat{p}_i = \underset{p \geqslant 0}{\text{argmin}} \left\{ \| C_i A p - f_i^c \|_2^2 \right\} \quad \forall \; i = 1, \ldots, K$$

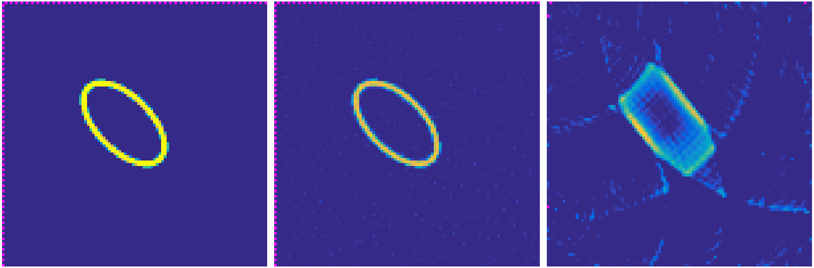

phantom | full data | sub-sampled (25x)

A 2D Example: Frame-by-Frame Total Variation

$$\hat{p}_i = \underset{p \geqslant 0}{\operatorname{argmin}} \left\{ \| C_i A p - f_i^c \|_2^2 + \lambda TV(p) \right\} \quad \forall \; i = 1, \ldots, K$$

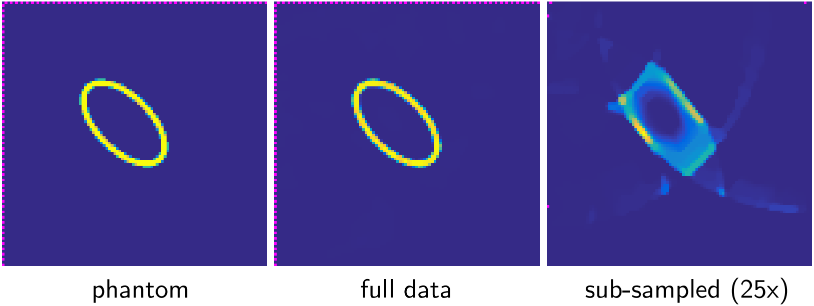

A 2D Example: TV-TV-L2

$$\left(\hat{P}, \hat{V}\right) = \operatorname*{argmin}_{P \geqslant 0, V} \left\{ \frac{1}{2} \sum_i^T \| C_i A \, p_i - f_i^c \|_2^2 \right.$$
$$\left. + \alpha TV(p_i) + \beta TV(v_i) + \gamma \| (p_{i+1} - p_i) + \nabla p_i \cdot v_i \|_2^2 \right\}$$

$\alpha = \beta = \lambda_{TV}$, $\gamma = 1$.

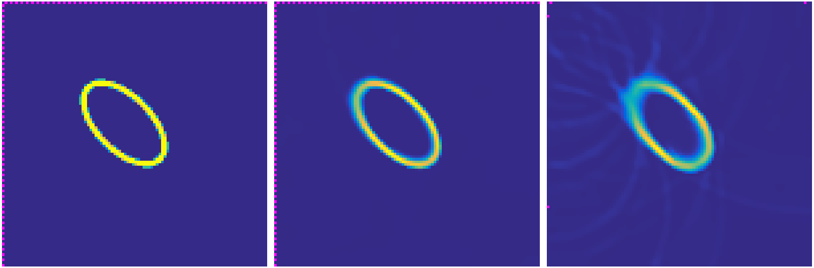

phantom | full data | sub-sampled (25x)

$$\left(\hat{P}, \hat{V}\right) = \underset{P \geqslant 0, V}{\operatorname{argmin}} \left\{ \frac{1}{2} \sum_{i}^{T} \| C_i A\, p_i - f_i^c \|_2^2 \right.$$
$$\left. + \alpha TV(p_i) + \beta TV(v_i) + \gamma \| (p_{i+1} - p_i) + \nabla p_i \cdot v_i \|_2^2 \right\}$$

$\alpha = \beta = \lambda_{TV}$, $\gamma = 0.1$.

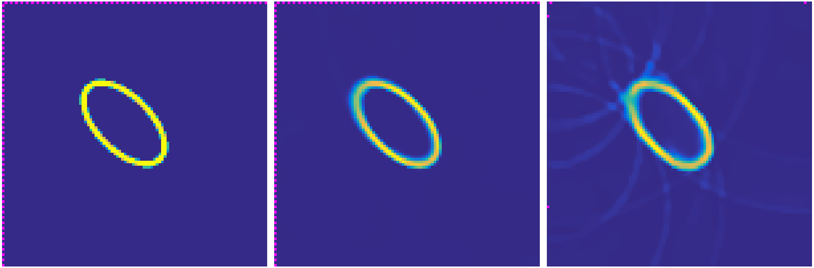

phantom　　full data　　sub-sampled (25x)

Artificially Sub-Sampled 3D Stop-Motion Data

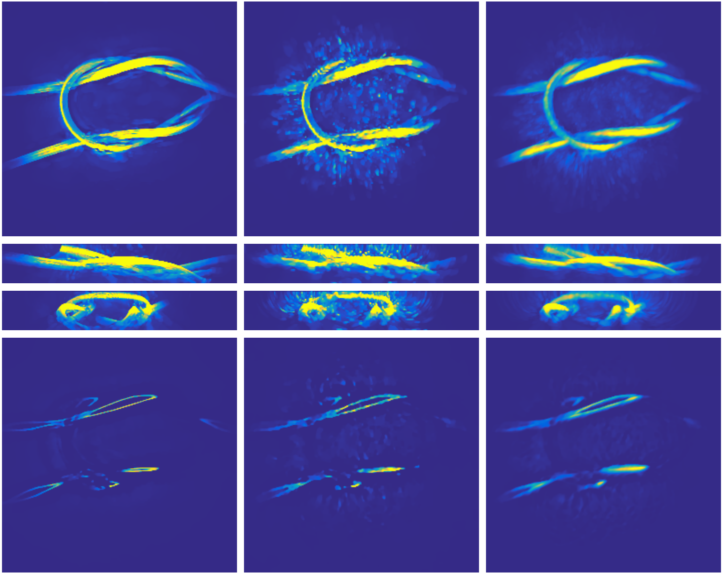

full data, TV-FbF

16x, TV-FbF

16x, TVTVL2

$\alpha, \beta = \lambda_{TV}, \gamma = 0.1$

Real Sub-Sampled Dynamic 3D Data (8 Beam Scanner)

sub-average over 8 frames

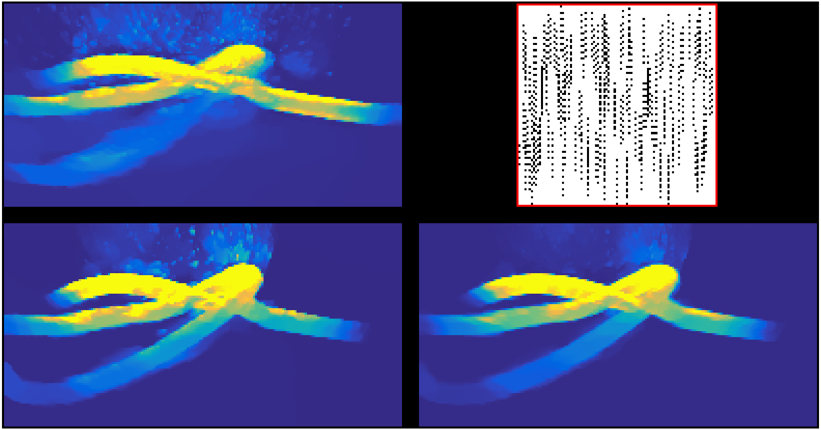

TV-FbF

TVTVL2, $\alpha = \beta = \lambda_{TV}$, $\gamma = 0.1$

Summary

UCL

Photoacoustic Tomography

- Imaging with laser-generated ultrasound ("hybrid imaging")
- High contrast for light-absorbing structures in soft tissue.
- Variety of promising (pre-)clinical applications.
- Two moderate inverse problems instead of one severely ill-posed.

Challenges of fast, high resolution 3D PA sensing:

- Nyquist requires several thousand detection points.
- Sequential schemes are slow.
- Crucial limitation for clinical, spectral and dynamical PAT.

Acceleration through sub-sampling:

- Exploit low spatio-temporal complexity to beat Nyquist.
- Acceleration by sub-sampling the incident wave field to maximize non-redundancy of data.
- Requires development of novel scanners.
- Demonstrated for Fabry-Pérot interferometer.

Results:

- Standard reconstruction methods fail on sub-sampled data.
- Adjoint PAT operator allows to use variational/iterative approaches.
- Sparse variational regularization/iterative non-convex projections give promising results for sub-sampled data.
- Demonstrated on simulated, experimental phantom and in-vivo data.

Challenges:

- Realizing this potential with experimental data requires
  - Model refinement/calibration.
  - Pre-processing to align data and model.
  - More suitable spatio-temporal constraints.
- Computationally extensive forward model.
- High dimensional, non-smooth, (non-)convex optimization.

- **Arridge, Beard, Betcke, Cox, Huynh, L, Ogunlade, Zhang, 2016**. *Accelerated High-Resolution Photoacoustic Tomography via Compressed Sensing*, *Physics in Medicine and Biology* 61(24).
- **Arridge, Betcke, Cox, L, Treeby, 2016**. *On the Adjoint Operator in Photoacoustic Tomography*, *Inverse Problems* 32(11).

cmic
Centre for Medical Image Computing

k-Wave

EPSRC
Engineering and Physical Sciences
Research Council

NVIDIA

We gratefully acknowledge the support of NVIDIA Corporation with the donation of the Tesla K40 GPU used for this research.

Thank you for your attention!

- **Arridge, Beard, Betcke, Cox, Huynh, L, Ogunlade, Zhang, 2016**. *Accelerated High-Resolution Photoacoustic Tomography via Compressed Sensing*, *Physics in Medicine and Biology* 61(24).

- **Arridge, Betcke, Cox, L, Treeby, 2016**. *On the Adjoint Operator in Photoacoustic Tomography*, *Inverse Problems* 32(11).

cmic Centre for Medical Image Computing

k-Wave

EPSRC Engineering and Physical Sciences Research Council

NVIDIA

We gratefully acknowledge the support of NVIDIA Corporation with the donation of the Tesla K40 GPU used for this research.

Iterative Schemes: Adjoint vs. Time Reversal

$$p^{k+1} = \Pi\left(p^k - \theta B\left(Ap^k - f\right)\right)$$

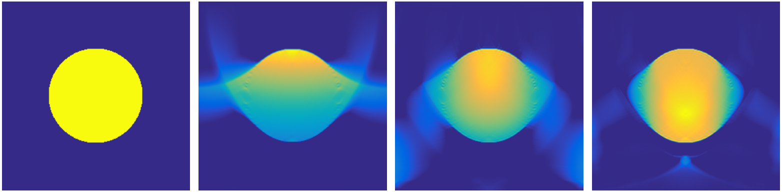

(a) Ground truth p_0 (b) TR (c) iTR (d) iTR+

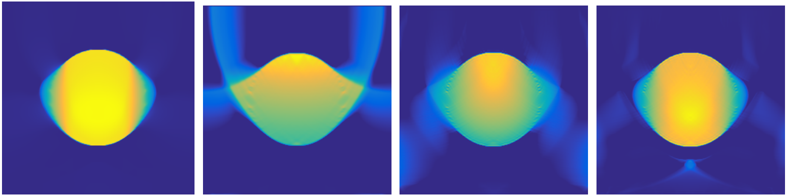

(e) TV+ (f) BP (g) LS (h) LS+

sensor on top; 2D slices at $y = 128$ through the 3D reconstructions.

For a proper, convex functional $\Psi : \mathbb{R}^n \longrightarrow \mathbb{R} \cup \{\infty\}$, the *Bregman distance* $D^p_\Psi(f,g)$ between $f, g \in \mathbb{R}^n$ for a subgradient $p \in \partial\Psi(g)$ is defined as

$$D^p_\Psi(f,g) = \Psi(f) - \Psi(g) - \langle p, f-g \rangle, \qquad p \in \partial\Psi(g)$$

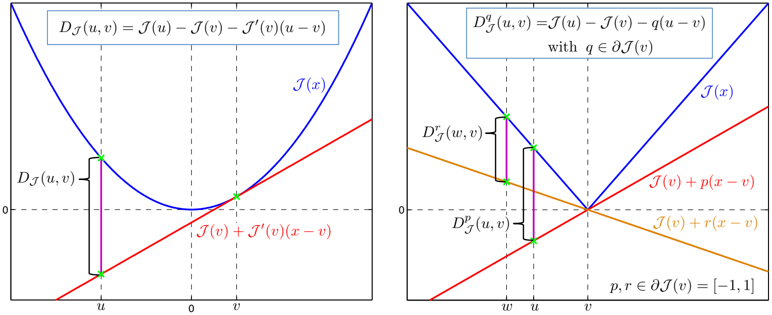

(a) $\mathcal{J}(x) = x^2$ (b) $\mathcal{J}(x) = |x|$

Basically, $D_\Psi(f,g)$ measures the difference between Ψ and its linearization in f at another point g

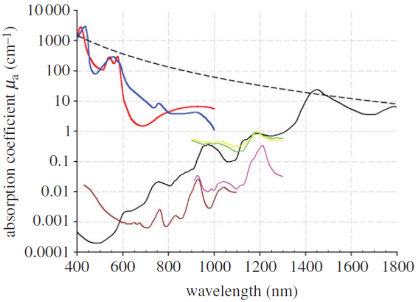

Figure 1. Absorption coefficient spectra of endogenous tissue chromophores. Oxyhaemoglobin (HbO_2), red line: (http://omlc.ogi.edu/spectra/hemoglobin/summary.html; 150 g l^{-1}), deoxyhaemoglobin (HHb), blue line: (http://omlc.ogi.edu/spectra/hemoglobin/summary.html; 150 g l^{-1}), water, black line [22] (80% by volume in tissue), lipid[a], brown line [23] (20% by volume in tissue), lipid[b], pink line [24], melanin, black dashed line (http://omlc.ogi.edu/spectra/melanin/mua.html; μ_a corresponds to that in skin). Collagen (green line) and elastin (yellow line) spectra from [24].

- High contrast between blood and water/lipid.
- Light-absorbing structures embedded in soft tissue.
- Gap between oxygenated and deoxygenated blood ⇝ functional imaging.
- Different wavelengths allow quantitative spectroscopic examinations.
- Use of contrast agents for molecular imaging.

from: **Paul Beard, 2011**. *Biomedical photoacoustic imaging*, *Interface Focus.*

- Up to now, conventional data was sampled at Nyquist rates in space and time (numerical phantoms were band-limited in space).
- In experiments, conventional data is usually already sub-sampled in space but over-sampled in time.
- Reconstruction on a finer spatial grid to exploit high frequency content of time series.

Example:

- Scan a 20mm×20mm with $\delta_x = 150\mu m$ (133×133 locations).
- Measured with temporal resolution of $\delta_t = 12ns \approx 83MHz$.
- Low-pass filtered to 20MHz.
- Reconstructing a signal limited to 20MHz with a sound speed of $1540 m\,s^{-1}$ would required $\delta_x = 38.5\mu m$ and $\delta_t = 25ns$.